Prolegomena to a hybrid Classical/Rydberg simulator for hadronization (QuPYTH)

Kenneth Heitritter,[1,2] Yannick Meurice,[1] and Stephen Mrenna[2]
[1] *The University of Iowa, Iowa City, IA 52242, USA*
[2] *Fermi National Accelerator Laboratory, Batavia, IL 60510, USA*
(Dated: February 16, 2023)

We present the classically simulated integration of a hadronization model, based on neutral Rydberg atoms, with the PYTHIA event generator. The real-time evolution of an interpreted charge-anticharge, in our Rydberg model, displays features similar to string-breaking - reminiscent of the Lund string fragmentation model used in PYTHIA for hadronization. We calculate the real-time evolution classically for a Rydberg simulator with up to 26 atoms. The behavior for increasing sites suggests that the model would be approaching semi-realistic hadron multiplicities using current QuEra hardware.

arXiv:2212.02476v2 [quant-ph] 15 Feb 2023

Introduction.— Programmable arrays of neutral atoms with highly excited Rydberg states present a significant new tool to study quantum many-body systems [1–7]. More generally, the idea of using analog platforms, like those constructed of Rydberg atoms, to simulate quantum systems has received a great deal of attention [8–21]. Recent work has found these Rydberg arrays can realize gauge theories in the form of the spin-$\frac{1}{2}$ truncated (1+1)-d Schwinger model [22], spin-$\frac{1}{2}$ (2+1)-d lattice gauge theories [23], and for the spin-1 Abelian-Higgs model [24]. Simplified lattice gauge theories and quantum spin chains [25–40] have been shown to display dynamical features related to QCD and the phenomenon of string-breaking.

Hadronization is the transition of quarks and gluons into hadrons, and is understood qualitatively from the confining properties of QCD. However, practical, first-principle predictions for hadronization are not currently available, and phenomenological models are used as a proxy when comparing field theory calculations to data. One such model, the Lund string model [41], is implemented in the widely-used high-energy event generator PYTHIA [42, 43]. The development of hadronization models has been identified as an avenue of great practical relevance for future tests of the Standard Model [44].

The goal of this work is to construct a configuration of Rydberg atoms that displays confinement, develop a model for carrying out hadronization, and integrate this Rydberg hadronization model with the PYTHIA event generator. This integration is not expected to match the phenomenological success of the current PYTHIA string model, but constitutes a proof-of-concept that quantum hardware can be integrated with classical event generation.

Lund string model review.— In the Lund string model, the effective linear potential between color charges gives rise to a color flux or vortex tube. To a first approximation, the tube is a 1+1-dimensional, massless, relativistic string with negligible transverse dimensions. Hadron spectroscopy indicates that such a string has energy per unit length $\kappa \approx 1$ GeV/fm.

As color-anticolor charges separate in spacetime, the potential energy stored in the string increases until it can produce a new quark-antiquark pair from vacuum fluctuations, splitting the original string into a string and a hadron. This breaking continues until the entire string is converted into hadrons. The hadron multiplicity, defined as the average number of hadrons produced from a string, predicted by PYTHIA is shown in Fig. 1.

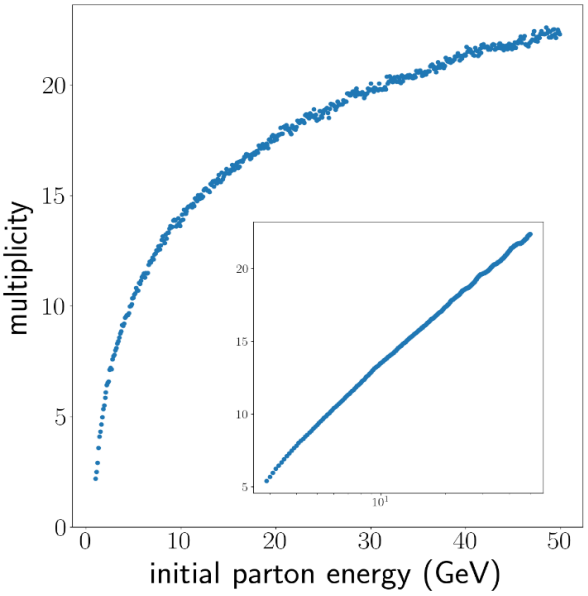


FIG. 1. Hadron multiplicity predictions with default PYTHIA hadronization from an initial $u\bar{u}$ pair. A primary goal for a hadronization model based on Rydberg atoms is to achieve a similar logarithmic behavior. Inset depicts the same data with a logarithmic x-axis and smoothing applied.

Rydberg dynamics.—The dynamics of Rydberg atom configurations is governed by the Hamiltonian

$$H = \frac{\Omega}{2}\sum_{j=1}\left(|g_j\rangle\langle r_j| + |r_j\rangle\langle g_j|\right) - \Delta\sum_{j=1} n_j + \sum_{j<k=1} V_{jk} n_j n_k \,, \quad (1)$$

where the sums are over all atoms. The Rydberg atoms represent qubits with ground states $|g\rangle$ and excited (Ry-

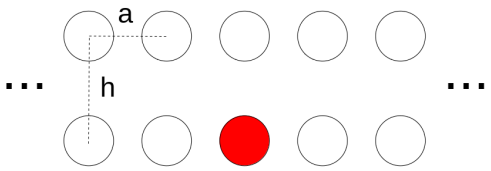


FIG. 2. Two-leg ladder arrangement of Rydberg atoms where h is the inter-rung spacing and a is the outer-rung (lattice) spacing. The ladder can be specified by an inverse aspect ratio $\rho = h/a$, and we work with $\rho = 2$ unless otherwise specified, whereas previous studies [24] have focused on $\rho \sim 0.4$. The red circle represents an excited atom, while the white circles correspond to ground states.

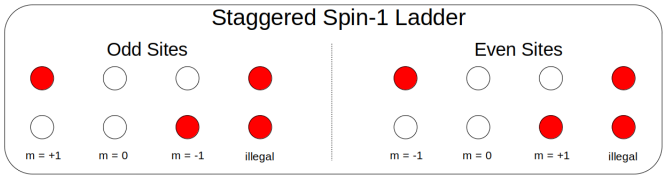


FIG. 3. State mapping for odd and even sites of a two-rung ladder. Red (white) circles denote excited (ground) states.

dberg) states $|r\rangle$. These states are coupled by the first term in the Hamiltonian, representing Rabi flipping with Rabi frequency Ω. The second term represents the global laser detuning, which varies the energy gap between the ground state $|g\rangle$ and excited state $|r\rangle$. Here, the operator $n_j \equiv |r_j\rangle\langle r_j|$, and the parameter Δ is called the detuning. The last term is the repulsive (van der Waals) interaction between excited atoms $|r\rangle$ with potential given by

$$V_{jk} = \frac{C_6}{|r_j - r_k|^6} \,, \tag{2}$$

where C_6 is the Rydberg interaction constant particular to the specific Rydberg state used.

In this work, we consider Rubidium-87, so that $|r\rangle = |70S_{1/2}\rangle$ and $C_6 = 862690 \times 2\pi$ MHz $\cdot\, \mu$m^6. The strong repulsive interaction Eq. (2) causes simultaneous excitations between neighboring atoms to become energetically prohibited. The radius at which this excitation-blocking effect becomes important is known as the Rydberg blockade radius and is defined to be the distance where

$$\frac{C_6}{R_b^6} = \Omega \,, \tag{3}$$

such that $R_b = (C_6/\Omega)^{1/6}$. We use $\Omega = 4\pi$ MHz and the previous value of C_6, unless otherwise stated, to yield $R_b = 8.692$ μm.

Two-leg ladder construction.—We study an arrangement of neutral Rydberg atoms that form a two-leg ladder as displayed in Fig. 2. Recently, this ladder arrangement has been shown to partially map to a spin-1 truncation of the Abelian-Higgs model for a specific set of parameters [24]. Here, we study the dynamics of the two-leg ladder without reference to particular model mapping and demonstrate that it displays features of confinement that suggesting string-breaking.

Single-rung.—We first describe the mapping between the state space of the ladder and that of a chain of spin-1 sites. A single rung of the ladder, composed of two neutral Rydberg atoms, has four basis states $|gg\rangle, |gr\rangle, |rg\rangle, |rr\rangle$. When two atoms are placed near each other, the Rydberg blockade, caused by the strong repulsion between excited states Eq. (2), results in an energetic exclusion of the doubly-excited $|rr\rangle$ state. Therefore, a single blockaded rung is effectively represented by only the three basis states $|gg\rangle, |gr\rangle, and |rg\rangle$, which can be mapped to a single-site spin-1 Hilbert space. We define the single-rung operator $\mathcal{O}_n$

$$\mathcal{O}_n \equiv (n_{top} - n_{bottom}) = E \,, \tag{4}$$

where E is the spin-1 field operator. We refer to this mapping as the field representation and demonstrate its action on the blockaded basis states:

$$\begin{aligned} \mathcal{O}_n |rg\rangle &\equiv E |+1\rangle = +1 |+1\rangle \\ \mathcal{O}_n |gr\rangle &\equiv E |-1\rangle = -1 |-1\rangle \\ \mathcal{O}_n |gg\rangle &\equiv E |0\rangle = 0 \,. \end{aligned} \tag{5}$$

Many-rung.—To create the two-leg ladder, we put two or more of the previously described single rungs together. If the single-rung state mapping is applied equivalently to each rung of the ladder, antiferromagnetic configurations are preferred. This happens because the excited states are repulsive, and so simultaneous diagonal (antiferromagnetic) excitations dominate over nearest-neighbor excitations. For our purposes, we want the lower-energy diagonal excitations to represent a constant $E = \pm 1$ configuration, so we stagger the interpretation of the single-site spin-1 mapping when applied to multiple rungs. The staggering means that we interpret even and odd sites oppositely by applying the previous spin-1 mapping on odd rungs, where the chain labeling starts at one, and multiply the mapping by -1 on even rungs to produce the mapping displayed in Fig. 3. As an operator mapping, the field representation picks up a site-dependent negative sign

$$\mathcal{O}_{n,j} \equiv (n_{\rm top} - n_{\rm bottom}) \times (-1)^{j+1} = E_j \tag{6}$$

so that it correctly implements the state staggering

$$\begin{aligned} \mathcal{O}_{n,1} |rg\rangle |gr\rangle &= E_1 |+1\rangle |+1\rangle = +1 |+1\rangle |+1\rangle \\ \mathcal{O}_{n,2} |rg\rangle |gr\rangle &= E_2 |+1\rangle |+1\rangle = +1 |+1\rangle |+1\rangle \\ \mathcal{O}_{n,2} |rg\rangle |rg\rangle &= E_2 |+1\rangle |-1\rangle = -1 |+1\rangle |-1\rangle \,. \end{aligned} \tag{7}$$

A charge representation can be defined via the application of Gauss' law

$$Q_{i,i+1} = E_{i+1} - E_i \,, \tag{8}$$

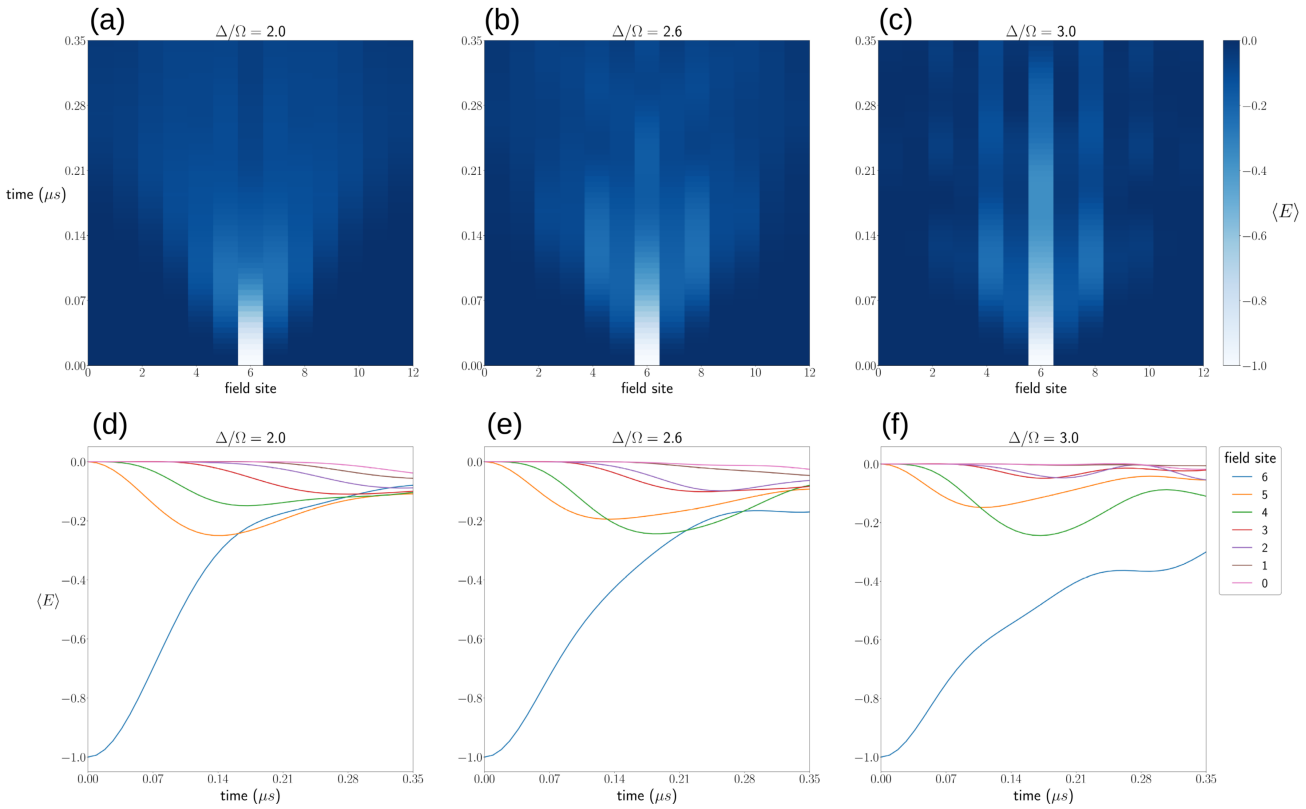


FIG. 4. Each column displays the field evolution (a-c) and field evolution of individual sites (d-f) for $R_b/a = 2.173$ and variable Δ/Ω increasing toward the right. For $\Delta/\Omega = 2.0$ (a), the initial field spreads nearly ballistically. As Δ/Ω is increased, the initial field spreads less readily and tends to form greater relative field densities at or close to the central site. It may be possible to interpret the initial excitation as having a higher (lower) energy for lower (higher) Δ/Ω. In this case, the initial excitation spreads easily when started with higher energy, but spreading is suppressed for a lower energy. Note that the field evolution in (a-c) depicts the average electric field and is, therefore, not exactly interpretable in terms of hadron multiplicity.

where we refer to $Q = \pm 1$ as charge/anticharge, respectively. The staggered interpretation can be seen to enforce Gauss' law, preventing E-field configurations like (...,+1,-1, ...) giving rise to $Q > 1$, via the Rydberg blockade constraint since these states have excited atoms as nearest-neighbors.

Observations of confinement-like behavior.— We conduct real-time evolution of the two-leg ladder, with staggered spin-1 mapping, using exact-diagonalization. Similar to previous studies of simulations for spin-chains [25, 32] and gauge theories [22, 27], we focus on the time-evolution of excitations, their probability maps as functions of model parameters, and entropy spreading to determine whether signatures of confinement are exhibited. Our results provide some credence to the claim that ladder configurations of Rydberg atoms present a new avenue to study confinement and may find applications to study real-time string-breaking.

Field/charge evolution.—We focus on the evolution of an initial state with a single excitation in its center, as shown in Fig. 2. This state can be prepared by applying a local detuning to a single central atom and then conducting an adiabatic ramp. Analysis of longer central excitations is deferred to a future paper. Aquila, a recent public device by QuEra Computing Inc., will soon be capable of these types of specific state preparation [45]. Examples of the single excitation state evolution for various parameters are displayed in Fig. 4, where the spin-1 staggered mapping has been implemented. The simulated evolution in Fig. 4 shows how the initial 100% probability central $E = -1$ field propagates outward symmetrically in a ballistic manner for lower Δ/Ω and generally becomes more constricted as Δ/Ω is increased.

Entropy evolution.—The dynamics of string-breaking is directly tied to confinement, and an observable of confinement is a reduction in the real-time spread of entropy. This behavior was first shown in terms of a generic CFT and numerically for the XY chain with a transverse magnetic field [46]. An analytic result was thereafter produced for the XY chain [47]. Since then, numerical studies of the Ising model with a transverse and longitudinal magnetic field [48], as well as implementation of the same model on a digital quantum computer [25], have continued to build evidence relating suppression of entropy spreading to confinement. We take a similar approach to substantiate our claim that the two-leg ladder on a Ryd-

berg atom architecture, with staggered spin-1 mapping, displays signatures of confinement in certain regions of its phase space. Calculation of entropy on a quantum computer is notoriously difficult, since it generally requires some form of state tomography. Recent studies have developed new experimental methods, using two-copy interferometry, that can reliably measure entropy for Rydberg atom systems [7, 49]. This opens a path to experimental verification of our entropy observations, which will be explored in future work.

We define the half-chain reduced density matrix $\rho_{\frac{1}{2}} = \mathrm{tr}_{\frac{1}{2}}(\rho)$, where the total density matrix is traced over half (horizontal direction) of the atomic ladder, excluding the central rung. Inclusion of the central rung was found to not significantly modify results. From the half-chain density matrix, we define the von Neumann entanglement entropy $S_e = -\mathrm{tr}\left(\rho_{\frac{1}{2}} \ln \rho_{\frac{1}{2}}\right)$. Selecting the maximum entropy over a finite time-evolution, we build a phase diagram Fig. 5 displaying structure similar to previous results [3]. We single out an outlined region of this phase diagram which displays confinement via its reduction in entropy spreading as a function of Δ/Ω.

Pythia *integration.*—We have displayed features reminiscent of confinement which are present in the two-leg ladder configuration of Rydberg atoms, which point toward its application to dynamical string-breaking, and, hence, a model of hadronization. With the onset of cloud-based quantum computing, and current availability of Rydberg atom architectures, such as QuEra Computing Inc.'s Aquila processor, we can begin real-world testing in the near-term. For the moment, Aquila is not able to prepare the initial state necessary for our current results, so we instead satisfy ourselves with a classical simulation of the true quantum system.

We here outline how our model can be integrated with existing event generators, using Pythia as an example.

1. Pythia produces parton-level configurations that are organized into color singlets of strings with (usually) quark-antiquark endpoints. The quark and antiquark pair can be boosted to their rest frame with equal and opposite three-momentum.

2. A linear interpolating function translates the energy of the quark-antiquark pair into the global detuning of the initial string configuration on the Rydberg simulator. Energy of the string is set by the Rydberg Hamiltonian Eq. (1) and therefore lower (higher) detuning corresponds to higher (lower) energy of the initial state.

3. The string state is prepared on the ladder configuration using local detuning and an adiabatic ramping procedure.

4. The string state is subjected to constant global Rabi flipping and detuning up until excitations reach the lattice boundary. At this time (t_f), the system state is measured. For the 13-rung ladder, this time is set to $t_f = 0.35\ \mu s$.

5. The measured state is post-processed according to the following steps:

   (a) The staggered spin-1 mapping transforms the ladder into the field representation. The measured state now appears as a number of strings, each with length ≥ 1.

   (b) The initial string energy is fractionally distributed to the measured strings such that the assigned energies are proportional to the string lengths.

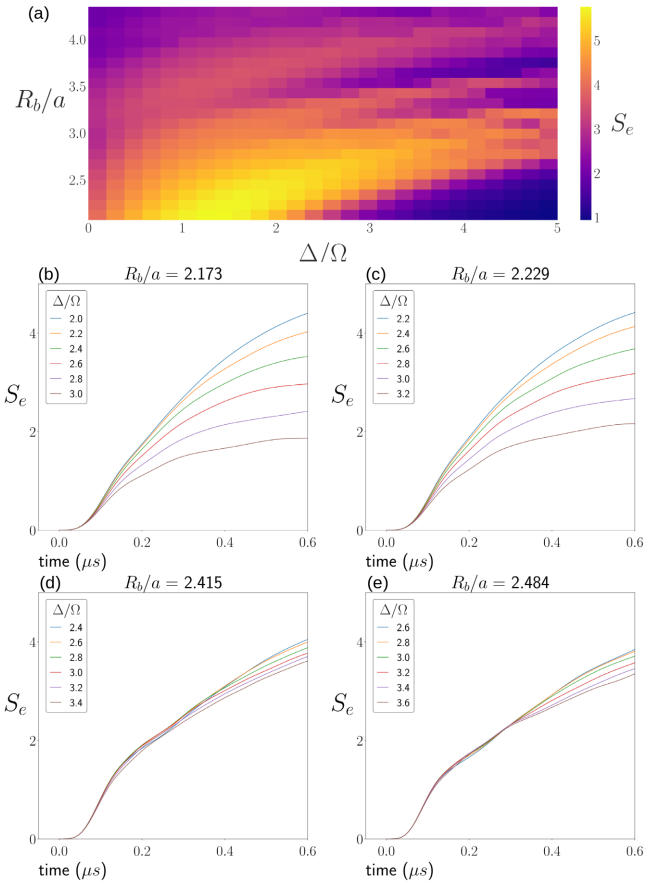


FIG. 5. (a) Maximum half-chain von Neumann entanglement entropy of a 13-rung ladder after evolving for $\Delta t = 1.8\ \mu s$. There is a maximum toward the bottom-left corner of the diagram and noticeable minima structure as one moves upward along the right side of the phase-space. These minima are likely due to the presence of Z_2, Z_3, and Z_4 ordered phases known to be present in the ground state of the Rydberg configuration [3]. (b-e) Real-time entropy evolution for a small range of parameters. All entropy evolutions approach asymptotic values at large times ($1.8\mu s$). (b) and (c) display clear suppression of entropy spreading as Δ/Ω is increased. Previous works have pointed toward this effect as a signature of confinement.

(c) The strings are converted to quark-antiquark pairs (mesons) separated by their corresponding string lengths using Gauss' law Eq. (8).

(d) Each meson is assigned a velocity by calculating the average velocity of its constituent quark-antiquark pair with respect to the initial string configuration.

(e) Each meson is assigned a mass using the previously calculated energy and velocity as inputs to the relativistic energy-mass relation.

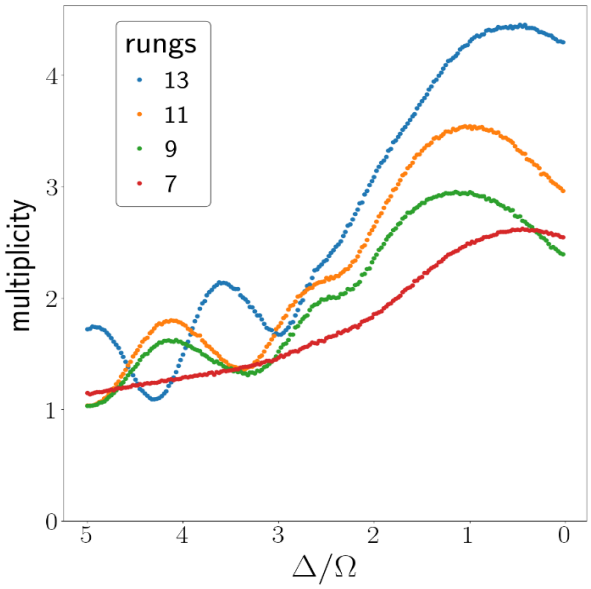


FIG. 6. Hadron multiplicity output of the Rydberg hadronization model for $R_b/a = 2.173$. Δ/Ω is plotted in decreasing order, since smaller values seem to be interpretable as having lower initial system energy and vice versa. The scaling is clearly not logarithmic as for PYTHIA in Fig. 1, but does display a monotonic increase in multiplicity for $\Delta/\Omega \in [2, 3]$, which displayed confining-like features. We see clearly, by looking at multiplicity output of smaller ladders, that number of rungs is the main limiting factor on the measured hadron multiplicity. The recently public Rydberg simulator, Aquila, has the ability to investigate ladders with 128 atoms.

These steps have been implemented with the Julia programming language using QuEra Computing Inc.'s open-source Rydberg simulator package Bloqade for the quantum computation and a custom branch of PYTHIA (available upon request). Example results of hadron multiplicity are shown in Fig. 6.

Conclusion.— We have shown that a two-leg ladder configuration of Rydberg atoms displays signatures of confinement previously pointed out in other models, and have shown how it can be used to implement a hadronization model within the PYTHIA event generator. The multiplicity output from the Rydberg hadronization does not currently mirror that of the Lund string model, but does monotonically increase for finite ranges of Δ/Ω. Studies of longer ladders, and at different aspect ratios, will likely be capable of producing more realistic multiplicities. Future studies may also be capable of probing the string tension, associated with our model, via interference experiments investigated in [50, 51]. Another potentially fruitful avenue is the determination of meson masses via entropy oscillations, as originally demonstrated in [48]. We hope that these results inspire others to further develop real-time simulations of QCD string-breaking, as advances in quantum hardware make such simulations feasible.

K.H. acknowledges support from the URA Visiting Scholars Program. K.H. and Y.M. are supported in part by the Dept. of Energy under Award Number DE-SC0019139. S.M. is supported in part by the U.S. Department of Energy, Office of Science, Office of High Energy Physics QuantISED program under the grants "HEP Machine Learning and Optimization Go Quantum", Award Number 0000240323, and "DOE QuantiSED Consortium QCCFP-QMLQCF", Award Number DE-SC0019219. This manuscript has been authored by Fermi Research Alliance, LLC under Contract No. DEAC02-07CH11359 with the U.S. Department of Energy, Office of Science, Office of High Energy Physics. This research was supported in part through computational resources provided by The University of Iowa, Iowa City, Iowa.

We thank Erez Zohar, Johannes Knaute, Johannes Zeiher, Debasish Banerjee, Fangli Liu, members of the QuLAT collaboration, and QuEra Computing Inc. for valuable comments and discussions.

[1] H. Bernien, S. Schwartz, A. Keesling, H. Levine, A. Omran, H. Pichler, S. Choi, A. S. Zibrov, M. Endres, M. Greiner, V. Vuletic, and M. D. Lukin, Nature **551**, 579 (2017).

[2] D. Barredo, V. Lienhard, S. de Léséleuc, T. Lahaye, and A. Browaeys, Nature **561**, 79 (2018).

[3] A. Keesling, A. Omran, H. Levine, H. Bernien, H. Pichler, S. Choi, R. Samajdar, S. Schwartz, P. Silvi, S. Sachdev, P. Zoller, M. Endres, M. Greiner, V. Vuletić, and M. D. Lukin, Nature **568**, 207 (2019).

[4] A. Browaeys and T. Lahaye, Nature Physics **16**, 132 (2020).

[5] P. Scholl, M. Schuler, H. J. Williams, A. A. Eberharter, D. Barredo, K.-N. Schymik, V. Lienhard, L.-P. Henry, T. C. Lang, T. Lahaye, A. M. Läuchli, and A. Browaeys, Nature **595**, 233 (2021).

[6] S. Ebadi, T. T. Wang, H. Levine, A. Keesling, G. Semeghini, A. Omran, D. Bluvstein, R. Samajdar, H. Pichler, W. W. Ho, S. Choi, S. Sachdev, M. Greiner, V. Vuletić, and M. D. Lukin, Nature **595**, 227 (2021).

[7] D. Bluvstein, H. Levine, G. Semeghini, T. T. Wang, S. Ebadi, M. Kalinowski, A. Keesling, N. Maskara, H. Pichler, M. Greiner, V. Vuletić, and M. D. Lukin, Nature **604**, 451 (2022).

[8] I. Bloch, J. Dalibard, and S. Nascimbène, Nature Physics **8**, 267 (2012).

[9] M. Lewenstein, A. Sanpera, V. Ahufinger, B. Damski, A. S. De, and U. Sen, Advances in Physics **56**, 243 (2007).

[10] J. I. Cirac, P. Maraner, and J. K. Pachos, Physical Review Letters **105**, 190403 (2010).

[11] E. Kapit and E. Mueller, Physical Review A **83**, 033625 (2011).

[12] Y. Kuno, S. Sakane, K. Kasamatsu, I. Ichinose, and T. Matsui, Physical Review D **95**, 094507 (2017).

[13] I. Danshita, M. Hanada, and M. Tezuka, Progress of Theoretical and Experimental Physics **2017** (2017), 10.1093/ptep/ptx108.

[14] J. Zhang, J. Unmuth-Yockey, J. Zeiher, A. Bazavov, S. W. Tsai, and Y. Meurice, Phys. Rev. Lett. **121**, 223201 (2018), arXiv:1803.11166 [hep-lat].

[15] Z. Davoudi, N. M. Linke, and G. Pagano, Physical Review Research **3**, 043072 (2021).

[16] Z. Davoudi, M. Hafezi, C. Monroe, G. Pagano, A. Seif, and A. Shaw, Physical Review Research **2**, 023015 (2020).

[17] C. Monroe, W. C. Campbell, L.-M. Duan, Z.-X. Gong, A. V. Gorshkov, P. Hess, R. Islam, K. Kim, N. Linke, G. Pagano, P. Richerme, C. Senko, and N. Y. Yao, Reviews of Modern Physics **93**, 025001 (2021).

[18] D. González-Cuadra, E. Zohar, and J. I. Cirac, New Journal of Physics **19**, 063038 (2017).

[19] M. Aidelsburger, L. Barbiero, A. Bermudez, T. Chanda, A. Dauphin, D. González-Cuadra, P. R. Grzybowski, S. Hands, F. Jendrzejewski, J. Jünemann, G. Juzeliunas, V. Kasper, A. Piga, S.-J. Ran, M. Rizzi, G. Sierra, L. Tagliacozzo, E. Tirrito, T. V. Zache, J. Zakrzewski, E. Zohar, and M. Lewenstein, Philosophical Transactions of the Royal Society A **380**, 20210064 (2022).

[20] C. Schweizer, F. Grusdt, M. Berngruber, L. Barbiero, E. Demler, N. Goldman, I. Bloch, and M. Aidelsburger, Nature Physics **15**, 1168 (2019).

[21] Y. Meurice, "Dynamical Gauge Fields on Optical Lattices: A Lattice Gauge Theorist Point of View," (2011).

[22] F. M. Surace, P. P. Mazza, G. Giudici, A. Lerose, A. Gambassi, and M. Dalmonte, Physical Review X **10** (2020), 10.1103/PhysRevX.10.021041.

[23] A. Celi, B. Vermersch, O. Viyuela, H. Pichler, M. D. Lukin, and P. Zoller, Physical Review X **10**, 021057 (2020).

[24] Y. Meurice, Phys. Rev. D **104**, 094513 (2021), arXiv:2107.11366 [quant-ph].

[25] J. Vovrosh and J. Knolle, Scientific Reports **11**, 11577 (2021).

[26] W. L. Tan, P. Becker, F. Liu, G. Pagano, K. S. Collins, A. De, L. Feng, H. B. Kaplan, A. Kyprianidis, R. Lundgren, W. Morong, S. Whitsitt, A. V. Gorshkov, and C. Monroe, Nature Physics **17**, 742 (2021).

[27] T. Pichler, M. Dalmonte, E. Rico, P. Zoller, and S. Montangero, Physical Review X **6**, 011023 (2016).

[28] S. Kühn, E. Zohar, J. I. Cirac, and M. C. Bañuls, Journal of High Energy Physics **2015**, 130 (2015).

[29] D. Banerjee, M. Dalmonte, M. Müller, E. Rico, P. Stebler, U. J. Wiese, and P. Zoller, Physical Review Letters **109**, 1 (2012).

[30] F. Hebenstreit, J. Berges, and D. Gelfand, Physical Review Letters **111**, 201601 (2013).

[31] V. Kasper, F. Hebenstreit, M. K. Oberthaler, and J. Berges, Physics Letters B **760**, 742 (2016).

[32] R. Verdel, F. Liu, S. Whitsitt, A. V. Gorshkov, and M. Heyl, Physical Review B **102**, 014308 (2020).

[33] B. Buyens, J. Haegeman, F. Hebenstreit, F. Verstraete, and K. Van Acoleyen, Physical Review D **96**, 114501 (2017).

[34] P. Sala, T. Shi, S. Kühn, M. Bañuls, E. Demler, and J. Cirac, Physical Review D **98**, 034505 (2018).

[35] D. Spitz and J. Berges, Physical Review D **99**, 036020 (2019).

[36] J. Park, Y. Kuno, and I. Ichinose, Physical Review A **100**, 013629 (2019).

[37] G. Magnifico, M. Dalmonte, P. Facchi, S. Pascazio, F. V. Pepe, and E. Ercolessi, Quantum **4**, 281 (2020).

[38] S. Notarnicola, M. Collura, and S. Montangero, Physical Review Research **2**, 013288 (2020).

[39] T. Chanda, J. Zakrzewski, M. Lewenstein, and L. Tagliacozzo, Physical Review Letters **124**, 180602 (2020), arXiv:1909.12657 [cond-mat].

[40] G. Pardo, T. Greenberg, A. Fortinsky, N. Katz, and E. Zohar, (2023), arXiv:2206.00685 [cond-mat, physics:hep-lat, physics:quant-ph].

[41] B. Andersson, G. Gustafson, G. Ingelman, and T. Sjöstrand, Physics Reports **97**, 31 (1983).

[42] C. Bierlich, S. Chakraborty, N. Desai, L. Gellersen, I. Helenius, P. Ilten, L. Lönnblad, S. Mrenna, S. Prestel, C. T. Preuss, T. Sjöstrand, P. Skands, M. Utheim, and R. Verheyen, (2022).

[43] T. Sjöstrand, S. Mrenna, and P. Skands, Journal of High Energy Physics **2006**, 026 (2006).

[44] J. M. Campbell, M. Diefenthaler, T. J. Hobbs, S. Höche, J. Isaacson, F. Kling, S. Mrenna, J. Reuter, S. Alioli, J. R. Andersen, C. Andreopoulos, *et al.*, "Event Generators for High-Energy Physics Experiments," (2022).

[45] "QuEra — Aquila," `https://www.quera.com/aquila`.

[46] P. Calabrese and J. Cardy, Journal of Statistical Mechanics: Theory and Experiment **2005**, P04010 (2005).

[47] M. Fagotti and P. Calabrese, Physical Review A **78**, 010306 (2008).

[48] M. Kormos, M. Collura, G. Takács, and P. Calabrese, Nature Physics **13**, 246 (2017).

[49] R. Islam, R. Ma, P. M. Preiss, M. E. Tai, A. Lukin, M. Rispoli, and M. Greiner, Nature **528**, 77 (2015).

[50] E. Zohar and B. Reznik, New Journal of Physics **15**, 043041 (2013).

[51] E. Zohar, J. I. Cirac, and B. Reznik, Physical Review Letters **110**, 055302 (2013).